J|A|C|S ARTICLES

Published on Web 12/10/2010

SWNT Nucleation from Carbon-Coated SiO_2 Nanoparticles via a Vapor−Solid−Solid Mechanism

Alister J. Page,[†] K. R. S. Chandrakumar,[†] Stephan Irle,*[,‡] and Keiji Morokuma*[,†,§]

Fukui Institute for Fundamental Chemistry, Kyoto University, Kyoto 606-8103, Japan, Institute for Advanced Research and Department of Chemistry, Nagoya University, Nagoya 464-8602, Japan, and Cherry L. Emerson Center for Scientific Computation and Department of Chemistry, Emory University, Atlanta, Georgia 30322, United States

Received October 6, 2010; E-mail: sirle@iar.nagoya-u.ac.jp (S.I.); morokuma@fukui.kyoto-u.ac.jp (K.M.)

Abstract: Since the discovery of single-walled carbon nanotubes (SWNTs) in the early 1990s, the most commonly accepted model of SWNT growth on traditional catalysts (i.e., transition metals including Fe, Co, Ni, etc.) is the vapor−liquid−solid (VLS) mechanism. In more recent years, the synthesis of SWNTs on nontraditional catalysts, such as SiO_2, has also been reported. The precise atomistic mechanism explaining SWNT growth on nontraditional catalysts, however, remains unknown. In this work, CH_4 chemical vapor deposition (CVD) and single-walled carbon nanotube (SWNT) nucleation on SiO_2 nanoparticles have been investigated using quantum-chemical molecular dynamics (QM/MD) methods. Upon supply of CH_x species to the surface of a model SiO_2 nanoparticle, CO was produced as the main chemical product of the CH_4 CVD process, in agreement with a recent experimental investigation [Bachmatiuk et al., *ACS Nano* **2009**, *3*, 4098]. The production of CO occurred simultaneously with the carbothermal reduction of the SiO_2 nanoparticle. However, this reduction, and the formation of amorphous SiC, was restricted to the nanoparticle surface, with the core of the SiO_2 nanoparticle remaining oxygen-rich. In cases of high carbon concentration, SWNT nucleation then followed, and was driven by the formation of isolated sp^2-carbon networks via the gradual coalescence of adjacent polyyne chains. These simulations indicate that the carbon saturation of the SiO_2 surface was a necessary prerequisite for SWNT nucleation. These simulations also indicate that a vapor−solid−solid mechanism, rather than a VLS mechanism, is responsible for SWNT nucleation on SiO_2. Fundamental differences between SWNT nucleation on nontraditional and traditional catalysts are therefore observed.

1. Introduction

The observation of carbon nanotubes (CNTs) in 1991[1] and the subsequent discovery of single-walled carbon nanotubes (SWNTs) in 1993[2,3] were landmark moments in the fields of nanoscience and nanotechnology. Since their discovery, the synthesis of SWNTs via transition-metal catalyzed chemical vapor deposition (CVD) and arc-discharge techniques has become a routine process on industrial scales. It has only been within the past decade that CNT synthesis on nontransition metal catalysts has been established.[4] The first such reports demonstrated the growth of CNTs from the sublimation decomposition of SiC,[5,6] and their formation from other allotropes of carbon.[7,8] The possibility of metal-free SWNT growth was also investigated theoretically on several occasions.[9−11] More recent experimental investigations have employed CVD on SiC, Ge, and Si nanoparticle catalysts.[12] The CVD synthesis of CNTs has also been demonstrated using carbon black substrates, nanodiamonds and fullerenes.[13,14] Other, atypical nanoparticles such as Al_2O_3 and ZrO_2 have also proved to be catalytically active in this context.[15,16] Since 2009, however, there has been a spate of investigations[17−21] demonstrating the CVD synthesis of CNTs on SiO_2 substrates.

The precise, atomistic mechanism by which CNT nucleation and growth proceeds on any nontraditional catalyst remains unknown. On the other hand, the vapor−liquid−solid (VLS) mechanism[22] is well-established in the context of traditional,

* To whom correspondence should be addressed.
† Kyoto University.
‡ Nagoya University.
§ Emory University.

(1) Iijima, S. *Nature* **1991**, *354*, 56.
(2) Iijima, S.; Ichihashi, T. *Nature* **1993**, *363*, 603.
(3) Bethune, D. S.; Klang, C. H.; de Vries, M. S.; Gorman, G.; Savoy, R.; Vazquez, J.; Beyers, R. *Nature* **1993**, *363*, 605.
(4) Homma, Y.; Liu, H.; Takagi, D.; Kobayashi, Y. *Nano Res* **2009**, *2*, 793.
(5) Kusunoki, M.; Rokkaku, M.; Suzuki, T. *Appl. Phys. Lett.* **1997**, *71*, 2620.
(6) Derycke, V.; Martel, R.; Radosavljevic, M.; Ross, F. M.; Avouris, P. *Nano Lett.* **2002**, *2*, 1043.
(7) Larciprete, R.; Lizzit, S.; Botti, S.; Cepek, C.; Goldoni, A. *Phys. Rev. B* **2002**, *66*, 121402.
(8) Koshio, A.; Yudasaka, M.; Iijima, S. *Chem. Phys. Lett.* **2002**, *356*, 595.
(9) Zhang, P.; Crespi, V. H. *Phys. Rev. Lett.* **1999**, *83*, 1791.
(10) Kawai, T.; Miyamoto, Y.; Sugino, O.; Koga, Y. *Phys. Rev. B* **2002**, *66*, 033404.
(11) Wang, Z.; Irle, S.; Zheng, G.; Kusunoki, M.; Morokuma, K. *J. Phys. Chem. C* **2007**, *111*, 12960.
(12) Takagi, D.; Hibino, H.; Suzuki, S.; Kobayashi, Y.; Homma, Y. *Nano Lett.* **2007**, *7*, 2272.
(13) Lin, J.-H.; Chen, C.-S.; Ma, H.-L.; Chang, C.-W.; Hsu, C.-Y.; Chen, H.-W. *Carbon* **2008**, *46*, 1619.
(14) Rao, F.; Li, T.; Wang, Y. *Carbon* **2009**, *47*, 3580.
(15) Liu, H.; Takagi, D.; Ohno, H.; Chiashi, S.; Chokan, T.; Homma, Y. *Appl. Phys. Exp.* **2008**, *1*, 014001.

iron-group metal catalyzed SWNT nucleation and growth.[23−25] According to the VLS mechanism, CNT growth is preceded by liquid-phase metal-carbide nanoparticles produced from the co-condensation of gas-phase metal and carbon atoms. Carbon super saturation in these metal-carbide precursors subsequently induces precipitation of carbon from the nanoparticle bulk to the surface, at which point the solid phase CNTs nucleate and grow. Among those reports of CNT synthesis on SiO_2 nanoparticles, few have attempted to propose a mechanism for CNT nucleation and growth. Huang et al. have speculated that "any materials with a suitable size may be effective catalysts for SWNT growth".[18] Such a statement is certainly inline with the observation that SWNTs can be grown even on natural minerals.[26] These authors also proposed that nanosized SiO_2 is molten at 1173.15 K. Presumably then, the VLS mechanism may be applicable in this case. Nevertheless, Huang et al. reported that no carbide whatsoever was observed in XPS spectra following SWNT growth. However, Liu et al.,[19] who also employed XPS methods, reported the presence of small amounts of carbon on the substrate. Similarly, Bachmatiuk et al.[17] observed that, during EtOH CVD synthesis of large-diameter carbon nanofibers (CNFs), the SiO_2 catalyst nanoparticles were carbothermally reduced, yielding SiC. These authors subsequently suggested that the nucleation of the yarmulke-like cap was preceded by the dissolution of gas-phase carbon into the SiO_2 nanoparticles, and the subsequent precipitation of this carbon from liquid/liquidlike SiC nanoparticles. In other words, it appeared that the VLS mechanism was responsible for the CVD growth of these CNFs. To add another piece to the puzzle, Homma et al. have shown that nontraditional covalent catalysts including Si,[12] SiC,[12] Al_2O_3,[15] SiO_2,[21] and nanodiamond[4] remain in the solid phase throughout CNT nucleation and growth. In such a scenario, a VLS-type mechanism is clearly unrealistic. Instead, CNT nucleation and growth was explained using a carbon-coated catalyst nanoparticle.

In this work, we present quantum-mechanical molecular dynamics (QM/MD) simulations of CH_4 CVD and SWNT nucleation on SiO_2 nanoparticles at 1200 K. In doing so, we will reveal the atomistic mechanisms of these nonequilibrium processes. The SWNT nucleation mechanism on SiO_2 will also be compared to the recently reported mechanisms observed using Fe and Ni nanoparticles.[27,28] It will be demonstrated herein that there are several fundamental differences separating SWNT nucleation on traditional catalysts (i.e., transition metals) from SWNT nucleation on SiO_2 catalysts. Most importantly, it will be shown that a vapor−solid−solid (VSS) mechanism, as opposed to a VLS mechanism, governs SWNT nucleation on SiO_2 catalysts.

2. Computational Methodology

Molecular dynamics calculations were performed by integrating the Newtonian equations of motion with the Velocity−Verlet algorithm ($\Delta t = 1.0$ fs). The nuclear temperature was controlled using a Nosé−Hoover chain thermostat[29] connected to the degrees of freedom of the system. The quantum chemical potential was generated using the SCC-DFTB method, in conjunction with a finite electronic temperature[30−32] ($T_e = 1500$ K). The latter assists dramatically in the convergence of the SCC equations, since the occupancy of each molecular orbital is described by a Fermi−Dirac distribution function of its energy. The occupancies of molecular orbitals close to the Fermi-level therefore varied continuously over the domain [0, 2]. Our group has used equivalent approaches extensively in describing the dynamics of SWNT nucleation and growth on a variety of transition-metal catalysts.[27,33−38] In the present context, the use of a nonzero T_e is considered to be essential, due to the prevalence of dangling C and Si bonds in the model system.

SiO_2-catalyzed SWNT nucleation has been simulated in this work at 1200 K using an isolated SiO_2-nanoparticle in a periodic $6.0 \times 6.0 \times 6.0$ nm^3 vacuum. The initial Si-terminated $Si_{63}O_{88}$ nanoparticle was obtained by truncating an extended β-quartz structure[39] and had approximate dimensions of $1.8 \times 1.5 \times 1.1$ nm^3. In the absence of a continued lattice framework this SiO_2 structure quickly relaxed, losing much of its original structural character and resembling instead an amorphous SiO_2 nanoparticle. This is illustrated in Figure S1 of the Supporting Information, which shows the SiO_2 nanoparticle after SCC-DFTB geometry optimization and 10 ps of thermal equilibration at 1200 K using SCC-DFTB/MD.

Liu et al.[20] have recently suggested that (due to the lack of catalytic activity of SiO_2) CH_4 molecules partially decompose pyrolytically *prior* to adsorbing on the SiO_2 surface. Concordantly, the SWNT nucleation algorithm employed in this work consists of 'shooting' randomly selected CH_x species ($x = 0-3$) representing pyrolytically decomposed methane fragments at the SiO_2 nanoparticle center-of-mass at intervals of 0.5 ps. Our group has used a similar shooting approach in previous simulations of transition-metal-catalyzed SWNT nucleation.[27] The value of x here is chosen according to a normalized Poisson distribution, and approximates the relative probabilities of successive dehydrogenation of CH_4 (i.e., the probability of producing CH_x, $P(CH_x)$, is such that $P(CH_3) > P(CH_2) > P(CH) \gg P(C)$). Following 10 ps of SCC-DFTB/MD, the removal of hydrogen from the model system was initiated at a rate of 4 H atoms/ps, until hydrogen was completely removed from the model system. Each hydrogen atom was selected randomly.

(16) Steiner, S. A.; Baumann, T. F.; Bayer, B. C.; Blume, R.; Worsley, M. A.; MoberlyChan, W. J.; Shaw, E. L.; Schlogl, R.; Hart, A. J.; Hofmann, S.; Wardle, B. L. *J. Am. Chem. Soc.* **2009**, *131*, 12144.
(17) Bachmatiuk, A.; Bornert, F.; Grobosch, M.; Schaffel, F.; Wolff, U.; Scott, A.; Zaka, M.; Warner, J. H.; Klingeler, R.; Knupfer, M.; Buchner, B.; Rummeli, M. H. *ACS Nano* **2009**, *3*, 4098.
(18) Huang, S.; Cai, Q.; Chen, J.; Qian, Y.; Zhang, L. *J. Am. Chem. Soc.* **2009**, *131*, 2094.
(19) Liu, B.; Ren, W.; Gao, L.; Li, S.; Pei, S.; Liu, C.; Jiang, C.; Cheng, H.-M. *J. Am. Chem. Soc.* **2009**, *131*, 2082.
(20) Liu, B.; Ren, W.; Liu, C.; Sun, C.-H.; Gao, L.; Li, S.; Jiang, C.; Cheng, H.-M. *ACS Nano* **2009**, *3*, 3421.
(21) Liu, H.; Takagi, D.; Chiashi, S.; Homma, Y. *Carbon* **2010**, *48*, 114.
(22) Saito, Y. *Carbon* **1995**, *33*, 979.
(23) Harris, P. J. F. *Carbon* **2007**, *45*, 229.
(24) Gavillet, J.; Thibault, J.; Stephan, O.; Amara, H.; Loiseau, A.; Ch, B.; Gaspard, J.-P.; Ducastelle, F. *J. Nanosci. Nanotechnol.* **2004**, *4*, 346.
(25) Irle, S.; Ohta, Y.; Okamoto, Y.; Page, A. J.; Wang, Y.; Morokuma, K. *Nano Res.* **2009**, *2*, 755.
(26) Kawasaki, S.; Shinoda, M.; Shimada, T.; Okino, F.; Touhara, H. *Carbon* **2006**, *44*, 2139.
(27) Ohta, Y.; Okamoto, Y.; Page, A. J.; Irle, S.; Morokuma, K. *ACS Nano* **2009**, *3*, 3413.
(28) Page, A. J.; Yamane, H.; Ohta, Y.; Irle, S.; Morokuma, K. *J. Am. Chem. Soc.*, in press.
(29) Martyna, G. J.; Klein, M. L.; Tuckerman, M. *J. Chem. Phys.* **1992**, *97*, 2635.
(30) Wagner, F.; Laloyaux, T.; Scheffler, M. *Phys. Rev. B* **1998**, *57*, 2102.
(31) Weinert, M.; Davenport, J. W. *Phys. Rev. B* **1992**, *45*, 13709.
(32) Wentzcovitch, R. M.; Martins, J. L.; Allen, P. B. *Phys. Rev. B* **1992**, *45*, 11372.
(33) Ohta, Y.; Okamoto, Y.; Irle, S.; Morokuma, K. *ACS Nano* **2008**, *2*, 1437.
(34) Ohta, Y.; Okamoto, Y.; Irle, S.; Morokuma, K. *J. Phys. Chem. C* **2009**, *113*, 159.
(35) Ohta, Y.; Okamoto, Y.; Irle, S.; Morokuma, K. *Carbon* **2009**, *47*, 1270.
(36) Ohta, Y.; Okamoto, Y.; Irle, S.; Morokuma, K. *Phys. Rev. B* **2009**, *79*, 195415.
(37) Page, A. J.; Irle, S.; Morokuma, K. *J. Phys. Chem. C* **2010**, *114*, 8206.
(38) Page, A. J.; Ohta, Y.; Okamoto, Y.; Irle, S.; Morokuma, K. *J. Phys. Chem. C* **2009**, *113*, 20198.
(39) Kihara, K. *Eur. J. Miner.* **1990**, *2*, 63.

Such an approach has recently been employed in the QM/MD investigation of giant fullerene[40] and polyaromatic hydrocarbon (PAH)[41] formation during the combustion of benzene and is, in effect, an attempt at mimicking the chemical removal of hydrogen from the system.

Significant chemical activity was observed during these simulations of SiO_2-catalyzed CH_4 CVD, in contrast to traditional, transition-metal-catalyzed SWNT nucleation (section 3). This resulted in constantly fluctuating populations of carbon on the SiO_2 nanoparticle during the early stages of the SWNT nucleation process. Constant surveillance of the SCC-DFTB/MD trajectories was necessary in order to ensure that sufficient amounts of carbon remained present on the SiO_2 nanoparticle. Recent experimental results indicate the existence of a carbon-coated solid nanoparticle during SWNT growth from nonmetal nanoparticles Ge,[12] Si,[12] SiC,[12] Al_2O_3,[15] SiO_2,[21] and nanodiamond.[4] To address this observation, we have employed three differing target carbon concentrations ([C]) on the SiO_2 nanoparticle, viz. 60, 100, and 140 carbon atoms (denoted as low, intermediate, and high concentration, respectively). The dependence of both the CH_4 CVD and SWNT nucleation processes on the carbon concentration may therefore be elucidated. That is, CH_x species were supplied to the surface of the SiO_2 nanoparticle until the number of carbon atoms reached one of these three concentrations, after which the system was simply annealed at constant temperature. In reality, due to the use of periodic boundary conditions, additional carbon-containing species were also adsorbed occasionally onto the SiO_2 surface. Thus, [C] in practice was slightly higher than originally intended. It is noted here that the SiO_2-catalyzed SWNT nucleation simulation reported in this work was replicated 10 times, trajectories that are referred to throughout this work using roman numerals 1−10, with subscripts denoting low, intermediate, and high [C].

3. Results and Discussions

3.1. Simulated CH_4 CVD on SiO_2 Nanoparticles. Simulations of CH_4 CVD on the model SiO_2 nanoparticle induced a surprisingly rich chemical process, in contrast to carbonaceous CVD processes on iron-group metal catalysts. In particular, the primary chemical product formed resulting from the interaction of CH_x with the SiO_2 was CO. Figure 1 shows the evolution of Trajectory 7_{low}, and the chemical activity observed during the first 35 ps. Figure 2 details the average chemical activity observed during the first 100 ps of the simulation, averaged over the 10 trajectories calculated for low, intermediate and high [C]. The corresponding structures of the SiO_2 nanoparticle after 100 ps are shown in Figures S1−S3 of the Supporting Information. It is immediate from Figure 1 that *the production of CO was the single dominant feature of this chemical process*. This observation is consistent with the recent experimental findings of Bachmatiuk et al.,[17] who observed the production of CO and SiO during CH_4 CVD on SiO_2. In contrast to these authors, however, no SiO was observed as a result of the interaction between CH_x and the SiO_2 nanoparticle in this work. Moreover, no Si was removed from the SiO_2 nanoparticle throughout the simulation in any trajectory. This was anticipated due to the use of different carbon feedstock (CH_4 instead of EtOH[17]), the disparate dimensions of the SiO_2 nanoparticles (ca. 2 nm instead of 10−50 nm[17]) and the use of a hydrogen atmosphere by Bachmatiuk et al.[17] Supplementary SCC-DFTB/MD simulations revealed that the SiO_2 model nanoparticle employed in this work was prone to disintegration in the presence of H_2. It is evident from Figure 1a, particularly during the earliest stages of the CVD simulation, that on several occasions CH_x species simply rebounded from the particle, despite their reactivity, underlining the catalytic inactivity of SiO_2.

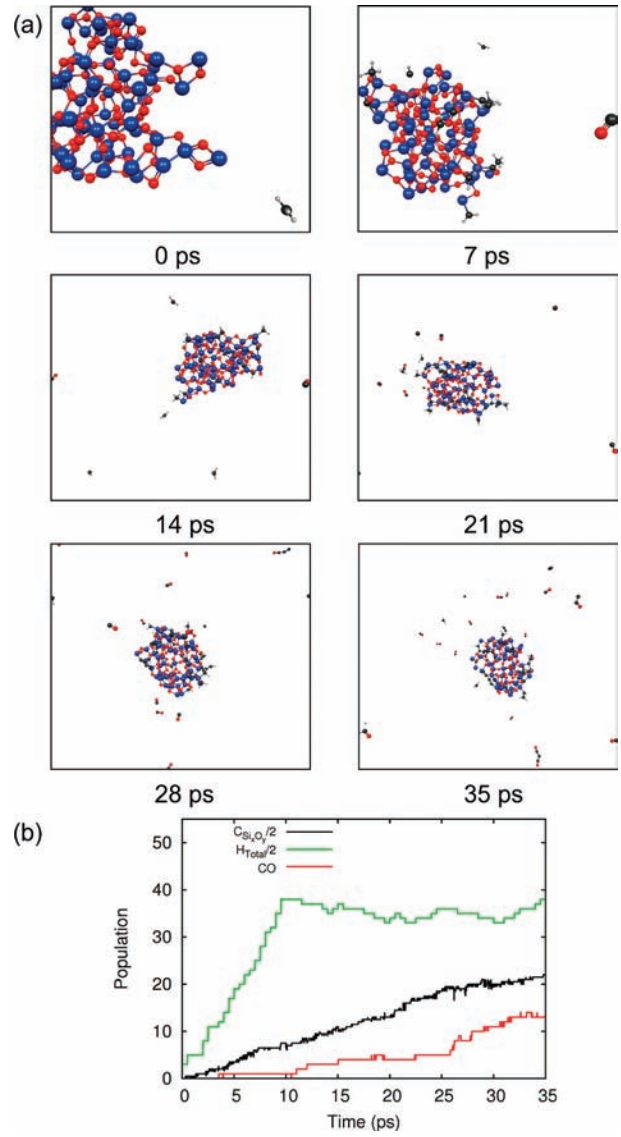

Figure 1. Evolution of Trajectory 7_{low}. (a) Snapshots during CVD simulation. Blue, red, black, and white spheres represent Si, O, C, and H atoms, respectively. (b) Total hydrogen (H_{total}), carbon residing on the SiO_2 nanoparticle ($C_{Si_xO_y}$), and total CO observed during CVD simulation.

Part b of Figure 1 and Figure 2 also illustrate that, during the initial stages of CVD, a significant amount of the carbon that initially interacts with the SiO_2 nanoparticle results in CO formation. In the case of Trajectory 7_{low}, it is evident that approximately 25% of all CH_x carbon supplied to the SiO_2 nanoparticle during the first 35 ps was released as CO. The average number of CH_x carbon atoms released as CO for low, intermediate and high [C] were 18.6, 22.2, and 24.4 (31%, 22%, and 17% of the respective target carbon concentrations). Consequently, there is a comparatively small amount of decomposed carbon density residing on/within the SiO_2 nanoparticle during this stage of the CVD process. The process of SWNT nucleation on SiO_2 nanoparticles is considered to be relatively inefficient in this respect, since much of the carbon decomposed onto the SiO_2 nanoparticle never participates in the process of SWNT nucleation itself. It is immediate from Figure 2a that for low [C] the point at which CH_x supply to the SiO_2 nanoparticle ceased (ca. 50 ps) coincided with the point at which the production of CO stopped. However, Figure 2b and 2c indicate that the point at which CO production ceased

(40) Saha, B.; Shindo, S.; Irle, S.; Morokuma, K. *ACS Nano* **2009**, *3*, 2241.
(41) Saha, B.; Irle, S.; Morokuma, K. *J. Chem. Phys.* **2010**, *132*, 224303.

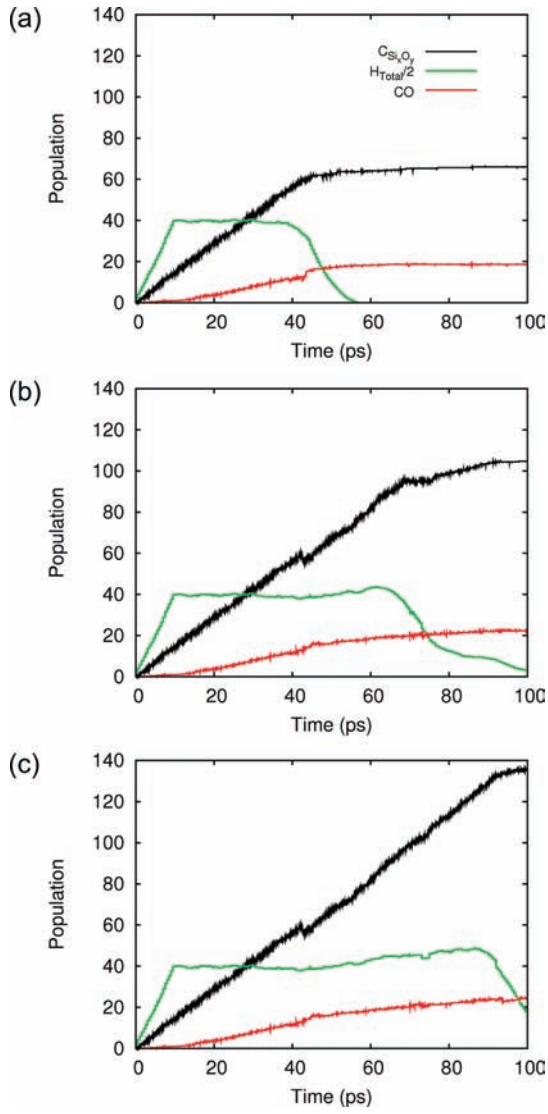

Figure 2. Average total hydrogen (H_{total}), carbon residing on the SiO_2 nanoparticle ($C_{Si_xO_y}$), and total CO observed during SCC-DFTB/MD simulations of CH_4 CVD for (a) low, (b) intermediate, and (c) high carbon concentration. All data averaged over 10 trajectories.

for intermediate and high [C] *preceded* the point at which CH_x supply was stopped. Instead, CO production ceased once the surface/subsurface region of the SiO_2 nanoparticle was saturated with carbon. Thus, the single factor governing the production of CO during CH_4 CVD on SiO_2 nanoparticles is the carbon concentration in the surface/subsurface region of the SiO_2 nanoparticle. It is also concluded from comparison of Figure 2a, 2b, and 2c that each CH_x moiety was only chemically active for the period immediately following its adsorption on the SiO_2 nanoparticle. That is, once a CH_x species was deposited onto the SiO_2 nanoparticle, it either reacted with SiO_2 oxygen, forming CO, or was sequestered into the surface/subsurface structure of the amorphous SiO_2 nanoparticle itself. A more detailed discussion of surface/subsurface saturation of carbon will be presented in subsequent sections.

3.2. Mechanism of CO Formation. We now turn to an explicit description of the CO production mechanism observed in our QM/MD simulations. This discussion pertains to results of low [C] simulations, although these results are entirely consistent with those of intermediate and high [C] simulations. This mechanism is featured in Figure 3 and movies S1a and S1b of the Supporting Information. In all cases of CO formation observed in this work, it was observed that *H abstraction (from the CO carbon) preceded the formation of CO itself*. The SiO_2 nanoparticle catalyst itself usually mediated this H abstraction. An example of such a process is shown in Figure 3a. In this case, a CH moiety bonded directly to a terminal oxygen atom of the SiO_2 nanoparticle after 3.96 ps of simulation. Naturally, the formation of this C−O bond weakened the existing Si−O−Si bridge structure on the surface of the catalyst. Following a further 0.08 ps, this Si−O−Si bridge structure gave way in favor of the Si−O−CH structure (4.04 ps). The OCH hydrogen atom was then almost immediately abstracted by a neighboring SiO_2 silicon atom (4.08 ps), at which point the CO moiety dissociated from the SiO_2 nanoparticle. Interestingly, the OCH hydrogen atom remained delocalized over the immediate region of the SiO_2 nanoparticle for a further 3−4 ps. During this time it interacted predominantly with two local silicon atoms. The separation of these two silicon atoms, via a conformational change of the SiO_2 nanoparticle, ultimately forced this hydrogen atom to bond to a single silicon atom.

Interestingly, H abstraction was also mediated by adjacent carbonaceous species deposited on the surface SiO_2 nanoparticle. An example illustrating this observation, shown in Figure 3b, begins with the addition of a CH moiety to the SiO_2 nanoparticle after 14.78 ps of simulation. In this case, the CH carbon initially formed an intermediate Si−O−C trigonal structure, before bonding to the same terminal oxygen atom of the SiO_2 nanoparticle. As observed in Figure 3a, the addition of this CH moiety weakened the existing Si−O−Si bond. In this case however, the Si−O−CH structure formed by the Si−O bond cleavage (14.96 ps) existed for 0.18 ps, slightly longer than the example discussed in Figure 3a. The OCH group formed at this point exhibited greater stability, persisting on the SiO_2 surface for another 0.36 ps. During this period, the OCH moiety formed exhibited greater vibrational and rotational freedom. This facilitated several dissociation attempts by the CO subunit. Nevertheless, only after a neighboring CH carbon abstracted the OCH hydrogen atom, at 15.32 ps, did the CO moiety finally dissociate from the SiO_2 nanoparticle.

The H abstraction/CO production process shown in Figure 3 not only illustrates the explicit role of the SiO_2 catalyst particle during the CH_4 CVD process, it also demonstrates a *natural hydrogen removal mechanism* during this process. The removal of hydrogen in this case is not only necessary for the formation of CO, but is also expected to make SWNT nucleation more favorable via the production of carbon dangling bonds (which in turn, due to their reactivity, readily contribute to the construction of an sp^2-hybrdized carbon network). This effect of hydrogen has previously been established during simulations of fullerene and polycyclic aromatic hydrocarbon formation from benzene combustion,[40] and Al/Fe-catalyzed SWNT nucleation.[42] Indeed, with respect to transition-metal-catalyzed SWNT nucleation, the exact mechanism by which hydrogen is removed from the carbon feedstock remains elusive to date. Our simulations here illustrate that the hydrogen removal process plays an important role at the atomic level and on atomic time scales.

3.3. Carbothermal Reduction of SiO_2 Nanoparticles. The production of CO precedes what can be considered to be the SWNT nucleation process itself. This was also concluded from a recent experimental study,[17] in which it was proposed that SiO_2 was carbothermally reduced to SiC, before C precipitation

(42) Eres, G.; Rouleau, C. M.; Yoon, M.; Puretzky, A. A.; Jackson, J. J.; Geohegan, D. B. *J. Phys. Chem. C* **2009**, *113*, 15484.

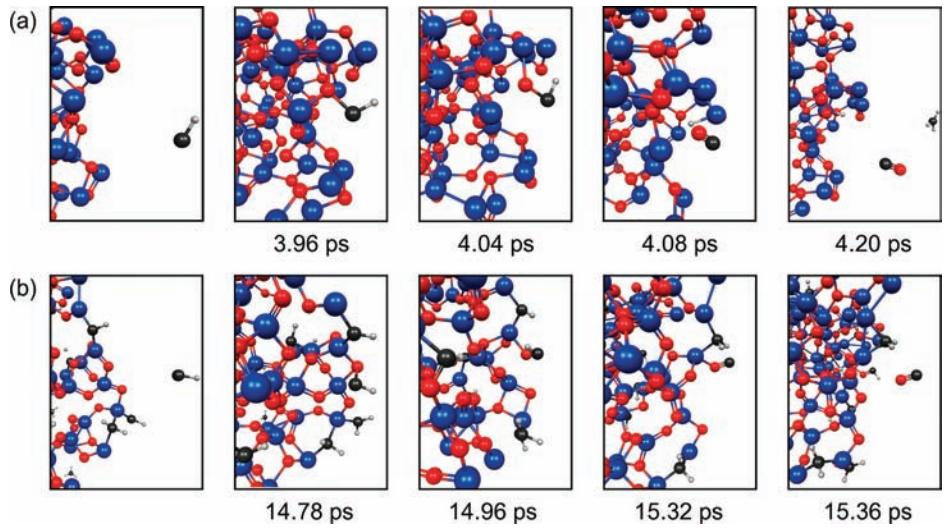

Figure 3. H-abstraction and CO production observed during CVD simulation (Trajectory 1_{low}). (a) Example of H-abstraction/CO production mediated by the SiO_2 catalyst. (b) Example of H-abstraction/CO production mediated by C adsorbed on SiO_2 catalyst. In both cases, H-abstraction precedes the formation and release of CO from the SiO_2 nanoparticle. Color conventions as in Figure 1. Time given with respect to the beginning of the simulation.

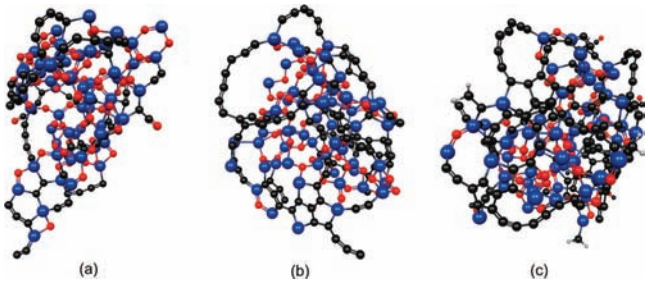

Figure 4. Carbothermal reduction of the SiO_2 nanoparticle observed in trajectories (a) 5_{low}, (b) $5_{intermediate}$, and (c) 5_{high}. In each case, SiO_2 reduction and amorphous SiC formation is limited to the surface/subsurface regions of the nanoparticle. Color conventions as in Figure 1.

took place, nucleating a SWNT cap fragment according to the VLS mechanism. The potential of carbon production via the decomposition of the SiC structure itself was also noted.[17]

The carbothermal reduction of SiO_2 during CH_4 CVD was also observed in the present work. It is evident from Figure 4 that, upon adsorption of CH_x onto the SiO_2 nanoparticle surface, those carbon atoms that were not expelled from the nanoparticle as CO remained on, or just below, the surface of the nanoparticle. Two primary differences from experimental observations[17] are therefore evident. First, as can be seen from Figure 4, the carbide structure formed from the carbothermal reduction of SiO_2 is clearly an amorphous one − no bulk SiC structure was formed as a result of the reduction process. Second, and perhaps more significantly, *the carbothermal reduction of SiO_2 by CH_x was limited to the surface/subsurface layers of the SiO_2 nanoparticle*. Thus, the core of the nanoparticle remained oxygen-rich in all computed trajectories. The localization of this carbon density in the SiO_2 surface/subsurface regions generally resulted in a large number of extended polyyne chains in/over the surface/subsurface regions of the SiO_2 nanoparticle. These chains accumulated and grew in length gradually during the course of the CVD process. The formation of these chains correlated with the carbothermal reduction of the amorphous SiO_2 nanoparticle, forming amorphous SiC. The sequestration of carbon into the SiO_2 nanoparticle and the formation of polyyne chains are very favorable processes in a thermodynamic sense, considering the strength of the Si−C/C−C interactions. The strength of the Si−C interaction (−6.88 eV/atom at the SCC-DFTB level of theory) also has ramifications with respect to the ability of SiO_2 to catalyze the SWNT nucleation and growth processes.

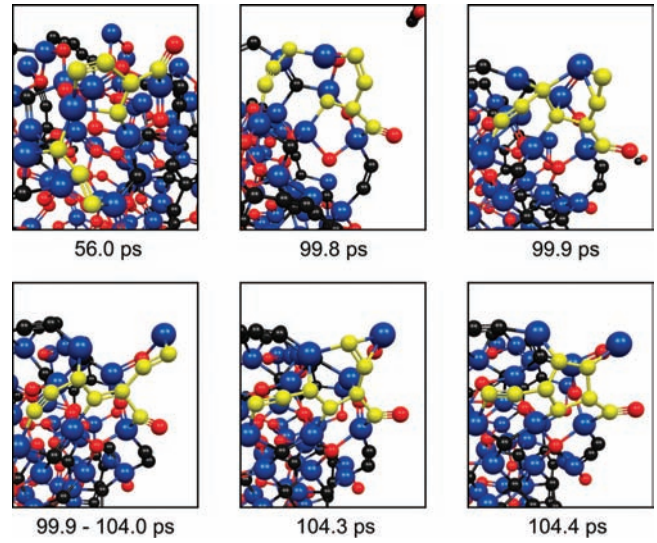

Figure 5. Conversion of free polyyne chains to constrained polyyne chains on the SiO_2 nanoparticle surface, observed in trajectory 10_{low}. In this case, two free polyyne chains located on the SiO_2 surface are converted to a constrained polyyne chain, after which a 5-membered carbon ring is formed. Color conventions as in Figure 1; yellow spheres are used to highlight polyyne chains referred to in the text.

Throughout the simulations presented in this work, the extended polyyne chains that were formed in the surface/subsurface layers of the SiO_2 nanoparticle generally took one of two forms. We denote these two forms here as free − those that exhibited terminal C−Si bonds only, and constrained − those that exhibited both terminal and nonterminal C−Si bonds. Both forms of polyyne chains are clearly visible in Figure 4. Upon thermal annealing, it was found that the populations of free and constrained polyyne chains fluctuated, with free polyyne chains being gradually converted into constrained polyyne chains. An example of this conversion, observed in trajectory 10_{low}, is illustrated in Figure 5 and movie S2 of the Supporting Information. The restricted vibrational and translational mobility of these surface polyyne chains is immediate from Figure 5.

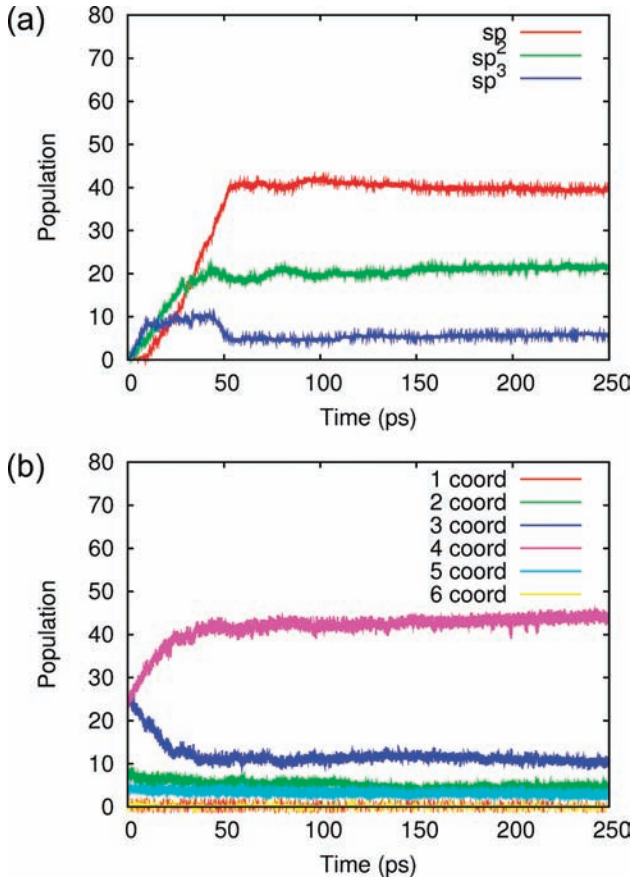

Figure 6. Evolution of the average coordination numbers of (a) carbon and (b) silicon atoms during SiO_2 catalyzed CH_4 CVD simulations at low carbon concentration. Only constituent atoms of the main SiO_2 cluster have been considered. All data averaged over 10 trajectories.

Remarkably, the polyyne chains in question (highlighted in Figure 5) remained essentially unchanged between 56.0 and 99.8 ps, due to the strong terminal C−Si bonds pinning the polyyne chains into position on the SiO_2 surface. After 99.9 ps a new C−C bond between the two surface polyyne chains was formed, at the expense of a terminal C−Si bond in one of the original polyyne chains. The remainder of the isomerization process of this new polyyne chain then took place relatively quickly. After 99.9 ps, the bridging C−Si−C structure was broken, a process that was induced by the configurational change of the catalyst surface itself. That is, the catalyst structure explicitly influenced the structure of the polyyne chain depicted in Figure 5. This phenomenon was also observed frequently in other trajectories for low, intermediate and high [C]. After 104.3 ps, an intermediate structure featuring a three-membered C−C−Si ring was formed. Understandably however, this structure was relatively unstable, lasting only 0.1 ps. The silicon atom present in the C−Si−C bridging structure was then displaced by these carbon atoms, resulting in the formation of a new C−C and hence a five-membered carbon ring at 104.4 ps.

The conversion of free polyyne chains to constrained polyyne chains was consistent with the evolution of the average coordination numbers of carbon and silicon atoms (residing on the main SiO_2 cluster). These average coordination numbers are shown in Figure 6 for the first 250 ps of CH_4 CVD using low [C]. After the supply of CH_x ceased (at ca. 50 ps) the populations of sp, sp^2, and sp^3 carbon atoms stabilized. However, during the 200 ps of thermal annealing that followed, a gradual decrease in the sp carbon population was observed. This decrease was accompanied by a simultaneous increase in the sp^2 carbon population. A concomitant increase in the number of 4-coordinated silicon was also observed during this period. This increase in the population of 4-coordinated silicon was attributed to the formation of new C−Si bonds in the SiO_2 nanoparticle surface.

The protracted time scale over which this polyyne isomerization process took place is testament to the strength of the Si−C interaction itself. This also constitutes a fundamental difference between the SiO_2-catalyzed SWNT nucleation mechanism, and that using Fe/Ni etc. It has recently been established[27,28,37,43] that the translational and vibrational mobility of polyyne chains on Fe and Ni nanoparticle catalyst surfaces dictates the mechanism and dynamics of SWNT nucleation and growth. This is in turn attributed primarily to the weaker carbon−catalyst interaction strengths (−1.78 eV/atom (Fe) and −1.06 eV/atom (Ni), using SCC-DFTB). Despite the slow production of sp^2 carbon on the SiO_2 surface, it was accelerated significantly at higher carbon concentrations. Therefore, *the saturation of the surface/subsurface region of the SiO_2 nanoparticle is necessary before an extended sp^2 network can be established.* This proposal will be corroborated in the subsequent section, which deals exclusively with the formation of such a network and subsequently SWNT nucleation. The differences between SWNT nucleation mechanisms observed using SiO_2 and those observed using transition-metal catalysts will also be elaborated upon in the subsequent section.

The conclusions drawn here regarding the extent of SiO_2 reduction are seemingly at odds with the experimental conclusions of Bachmatiuk et al.,[17] but are consistent with the carbon-coated nanoparticle hypothesis of Homma et al.[4] We suspect that the differences in the extents of catalyst reduction are closely related to the respective sizes of the SiO_2 nanoparticles. In particular, the particles employed by Bachmatiuk et al.[17] during the synthesis of carbon nanofibers were far larger, whereas the particles used by the other groups had catalyst size distributions comparable the size of our model SiO_2 particle. The applicability of a VLS-type mechanism in the case of SiO_2 catalysts seems questionable, for two reasons. First, all carbon atoms adsorbed onto the SiO_2 nanoparticle in this work remained in the surface/subsurface regions of the nanoparticle, thus making precipitation of this carbon impossible. Second, the restricted vibrational/translational mobility of the subsurface/surface polyyne chains (which represent the majority of the adsorbed carbon) indicates that diffusion/precipitation of carbon over/through the SiO_2 nanoparticle is an energetically unfavorable process. Additionally, the nanoparticles shown in Figure 4 exist in the solid state throughout the SWNT nucleation process. This was concluded following consideration of the Lindemann index.[44] The Lindemann index of the SiO_2 nanoparticle employed here remained below 0.05 throughout all trajectories, irrespective of [C]. This was well below the accepted threshold[45−47] (0.10−0.15) signifying the solid−liquid phase transition. It is proposed therefore that *SWNT nucleation on SiO_2 nanoparticles is governed by a VSS-type mechanism, as opposed to a VLS-type mechanism.* Such a mechanism for CNT growth seems atypical. However, the VSS mechanism has been employed to describe the growth of a variety of inorganic nanowires (including

(43) Page, A. J.; Minami, S.; Ohta, Y.; Irle, S.; Morokuma, K. *Carbon* **2010**, *48*, 3014.
(44) Lindemann, F. A. *Phys. Z.* **1910**, *11*, 609.

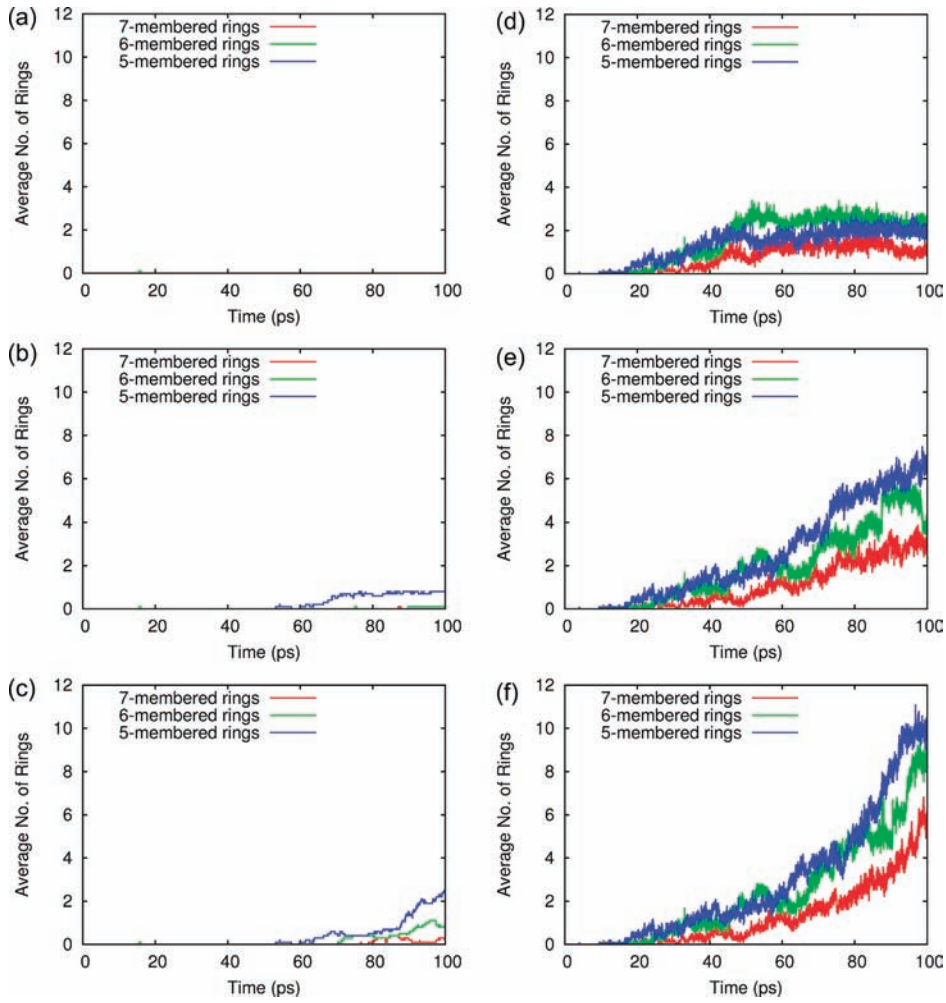

Figure 7. Average carbon only rings and carbon−silicon rings formed during SWNT nucleation on SiO_2. Carbon only rings are shown in (a), (b), and (c) for low, intermediate and high [C], respectively. Carbon−silicon rings are shown in (d), (e), and (f) for low, intermediate and high [C], respectively. All data averaged over 10 trajectories.

GaAs,[48] Si,[49] and ZnO[50]). These simulations also show that the fact that oxygen has no conceivable function in any stage during SiO_2-catalyzed SWNT nucleation. It is possible, therefore, that the atomistic mechanisms of SWNT nucleation using SiO_2, SiC, and Si nanoparticles are indistinguishable (i.e., catalyst-independent). Simulations aimed at addressing this possibility are presently being performed within our group.

3.4. SiO_2−Catalyzed SWNT Nucleation Mechanism. We now turn to a discussion of the explicit mechanism of SiO_2-catalyzed SWNT nucleation observed in our QM/MD simulations. SWNT nucleation on SiO_2 was defined by the creation of ring structures composed of carbon atoms. However, C−Si composite ring structures were also prominent during the nucleation process, as shown in Figure 7, indicating that the SiO_2 surface may play an explicit role in SWNT nucleation (as opposed to transition-metal catalysts). It is also evident that there was little, if any, preference between 5- and 6-membered C−Si ring productions during the early stages of SWNT nucleation, irrespective of [C]. The extent of C−Si ring production was proportional to the carbon concentration, as one might expect. Interestingly, active C−Si ring production using low [C] was only observed during the period of carbon adsorption. This observation is concomitant with the relationship between carbon adsorption and the chemical activity discussed previously. Figure 7a, 7b, and 7c show that carbon rings were only produced during intermediate and particularly high [C] simulations. Admittedly, carbon ring production was observed at low [C] over longer time scales (Figure S4 of the Supporting Information). However, this was limited to the production of a single ring in trajectory 10_{low} and so is not considered to constitute SWNT nucleation. Figure 7 also indicates that there is a distinct preference for 5-membered carbon ring production during SWNT nucleation on SiO_2. Such preferential 5-membered ring formation has also been observed during SWNT nucleation on Fe and Ni nanoparticles.[27,28] This preference is attributed to the high positive curvature of the catalyst nanoparticles in both cases.

An explicit example of SWNT nucleation, observed in trajectory 10_{high}, is depicted in Figure 8 and movie S3 of the Supporting Information. After 75.0 ps, a single 6-membered carbon ring was formed via a mechanism requiring numerous Si−C ring isomerizations. During the following 15 ps, this

(45) Borjesson, A.; Curtarolo, S.; Harutyunyan, A. R.; Bolton, K. *Phys. Rev. B* **2008**, *77*, 115450.
(46) Ding, F.; Bolton, K.; Rosen, A. *Eur. Phys. J. D* **2005**, *34*, 275.
(47) Shibuta, Y.; Suzuki, T. *Chem. Phys. Lett.* **2007**, *445*, 265.
(48) Persson, A. I.; Larsson, M. W.; Stenstrom, S.; Ohlsson, B. J.; Samuelson, L.; Wallenberg, L. R. *Nat. Mater.* **2004**, *3*, 677.
(49) Wen, C. Y.; Reuter, M. C.; Tersoff, J.; Stach, E. A.; Ross, F. M. *Nano Lett.* **2009**, *10*, 514.
(50) Campos, L. C.; Tonezzer, M.; Ferlauto, A. S.; Grillo, V.; Magalhães-Paniago, R.; Oliveira, S.; Ladeira, L. O.; Lacerda, R. G. *Adv. Mater.* **2008**, *20*, 1499.

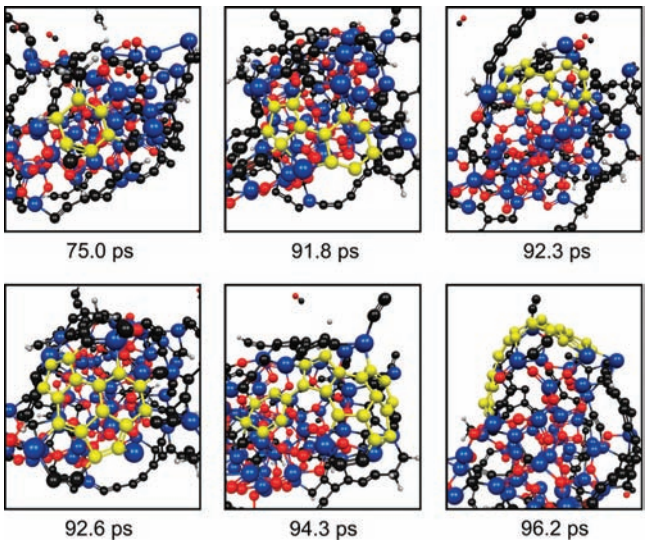

Figure 8. Successive carbon ring formations observed during SWNT nucleation on SiO_2 (trajectory 1_{high}). Color conventions as in Figure 1, yellow spheres are used to newly added carbon rings in the SWNT cap fragment.

6-membered ring was transformed into a 7-membered ring at 80.8 ps, due to an encroaching carbon atom in an adjacent 3-membered ring. Subsequent events of ring formation, each occurring at 91.8, 92.3, 92.6, 94.3, and 96.2 ps, resulted from the coalescence of adjacent polyyne chains adsorbed on the SiO_2 surface. The SWNT nucleation mechanism observed here was therefore dramatically different to that observed on Fe and Ni nanoparticles.[27,28] For example, the latter always features the formation of a Y-shaped polyyne junction, from which a 5-membered ring is formed. The vibrational motion of polyyne chains that extend from this 5-membered ring nucleus then drives subsequent ring condensation. This is not the case in the present work because of the restricted vibrational/translational motion of the adsorbed polyyne chains. Instead, the configurational dynamics of the SiO_2 surface region dictate ring condensation here. A much higher surface density of carbon is therefore required before SWNT nucleation is observed. This conclusion is consistent with a phenomenon we found commonly at intermediate and high carbon concentrations, namely the formation of isolated sp^2-carbon islands, often consisting of only one carbon ring, or a single conjugated ring structure. The existence of these islands is again consistent with the carbon-coated nanoparticle hypothesis of Homma et al.[4] The kinetics of SWNT growth on SiO_2 is also anticipated to be inferior to that observed on transition-metal catalysts. In the majority of computed trajectories using intermediate and high [C], the carbon rings formed were generally isolated from each other. In addition, the rates at which these sp^2-carbon islands were formed were prohibitively slow, due to the low vibrational and translational mobility of the constituent polyyne chains on the SiO_2 surface. Consequently, a realistic time scale for SWNT growth is likely to be significantly larger than those employed here (i.e., on the order of nanoseconds or longer). This is consistent with experimental data − for example, experimental growth rates using Al_2O_3 and SiO_2 are ca. 1−3 orders of magnitude slower compared to those using Fe.[4,20] The explicit atomistic mechanism of continued SWNT growth is presently unknown. Simulations to elucidate this mechanism are currently being performed in our group.

4. Conclusions

We have reported here the atomistic mechanism of SWNT nucleation on SiO_2 catalyst nanoparticles, based on QM/MD simulations of CH_4 CVD. In agreement with experiment,[17] CO was produced as the main chemical product of this CH_4 CVD process. The production of CO in this case, and the nucleation of CNTs in general, necessitate the abstraction of atomic hydrogen from the CO carbon. We have therefore observed the mechanism by which this removal takes place in the case of SiO_2 catalysts. The production of CO during CH_4 CVD resulted in the carbothermal reduction of the SiO_2 nanoparticle, resulting in a catalyst nanoparticle consisting of a SiO_2 core surrounded by an amorphous SiC shell. The first stage of the SWNT nucleation process featured the coalescence of carbon atoms on the SiO_2 surface, resulting in the formation of extended polyyne chains. At higher carbon concentrations, the isomerization of these polyyne chains resulted in the formation of isolated sp^2-carbon networks on the SiO_2 surface via ring condensation, and, ultimately, the formation of a SWNT cap structure. The surface saturation of the SiO_2 nanoparticle was a necessary prerequisite for SWNT nucleation. This is consistent with the hypothesis of a carbon-coated nanoparticle precursor.[4] The SiO_2/SiC nanoparticle remained in the solid phase throughout the nucleation process. Elements of SiO_2-catalyzed SWNT nucleation are therefore irreconcilable with those of a VLS-type mechanism. Instead, it is concluded that SiO_2-catalyzed SWNT nucleation proceeds according to a VSS mechanism, and so is comparable to the growth of a number of other inorganic nanostructures.[48−50] Consequently, it is evident that the processes of SWNT nucleation on SiO_2 and traditional catalysts (such as Fe and Ni[27,28]) differ at the most fundamental level.

Acknowledgment. This work was in part supported by a CREST (Core Research for Evolutional Science and Technology) grant in the Area of High Performance Computing for Multiscale and Multiphysics Phenomena from the Japanese Science and Technology Agency (JST). Computer simulations were performed using The Academic Center for Computing and Media Studies (ACCMS) at Kyoto University. S.I. acknowledges the Program for Improvement of Research Environment for Young Researchers from Special Coordination Funds for Promoting Science and Technology (SCF) commissioned by the Ministry of Education, Culture, Sports, Science and Technology (MEXT) of Japan for support.

Supporting Information Available: Structures of trajectories 1_{low}−10_{low}, $1_{intermediate}$−$10_{intermediate}$, and 1_{high}−10_{high} following 100 ps of SCC-DFTB/MD simulation; .mp4 movies showing CO production during CH_4 CVD simulation; .mp4 movie showing the polyyne conversion mechanism observed in trajectory 10_{low}; figures showing carbon ring formation and carbon/silicon coordination numbers for 250 ps at low carbon concentration; .mp4 movie showing the SWNT cap formation mechanism observed in trajectory 1_{high}. This material is available free of charge via the Internet at http://pubs.acs.org.

JA109018H